Journal of chemical & engineering data

Article

pubs.acs.org/jced

Structure of Ice in Confinement: Water in Mesoporous Carbons

Kamila Domin,[†,‡] Kwong-Yu Chan,[§] Hoi Yung,[§] Keith E. Gubbins,[∥] Marcin Jarek,[‡] Angelina Sterczynska,[†] and Malgorzata Sliwinska-Bartkowiak*[,†]

[†]Faculty of Physics, Adam Mickiewicz University, Umultowska 85, 61-614 Poznan, Poland

[‡]NanoBioMedical Centre in Poznan, Umultowska 85, 61-614 Poznan, Poland

[§]Department of Chemistry, University of Hong Kong, Pokfulam Road, Hong Kong, China

[∥]Department of Chemical & Biomolecular Engineering, North Carolina State University, Raleigh, North Carolina 27695, United States

ABSTRACT: In this study, the structure of nanoconfined ice and its behavior during the melting process have been investigated. For this purpose, deionized water was inserted into the pores of the ordered carbon structures CMK-3 and CMK-8 having pores of different diameters. The first set of experiments was performed using differential scanning calorimetry (DSC), from which the melting transition temperature of the confined ice was determined. In order to investigate the structure of ice formed inside the mesopores, wide-angle X-ray scattering was used. The measurements were performed at temperatures from 173 K up to and above the pore melting point for each system. The results of the XRD experiments showed features characteristic of both hexagonal, I_h, and cubic, I_c, ice at temperatures below the melting point. The structure of the confined ice corresponds to disordered stacking ice layers, ice I_{sd}, and our results agree well with recent simulations of X-ray diffraction of such ice crystals by Murray and co-workers.

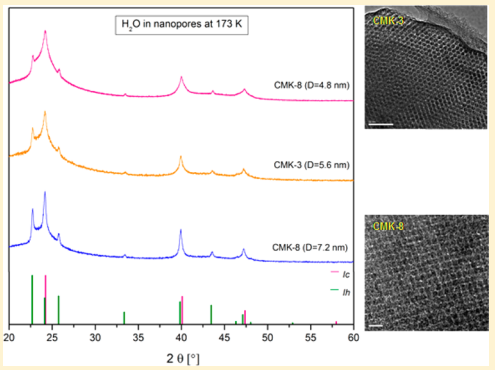

INTRODUCTION

Mesoporous materials find various applications in technological, pharmaceutical, medical, ecological, and many others areas due to their unique adsorptive properties. Especially ordered mesoporous carbon structures fabricated with the nanocasting method have attracted much attention due to their narrow pore size distribution, high surface area, thermal stability, and the possibility of controlling (to some extent) the shape and size of the pores, in order to fulfill demands in certain applications. In this work we report a study of ice structure in CMK mesoporous carbons, which can be prepared having a range of pore sizes.

Substances which are confined inside narrow cavities, exhibit different kinds of behavior than in bulk. This phenomenon occurs due to the size effect, wall forces, and competition between fluid−fluid and fluid−wall interactions. For example, the properties of confined water can be very different from those of bulk water, and this phenomenon is not yet well understood. One of the most interesting and well-known effect of nanoconfinement is depression in the freezing temperature of water.[1−8] It was also shown that water confined in very small pores (of diameter less than 1.6 nm) does not freeze even at temperatures lower than 130 K.[9] A further aspect of nanoconfinement is the formation of novel ice structures inside nanopores. Numerous investigations of water confined in porous matrices (silica and carbon) have been performed,[6,7,10−14] using a variety of methods, and have provided convincing evidence for the formation of ice structures other than the hexagonal structure found in bulk ice at ambient conditions. It has been shown that water confined in silica nanopores crystallizes to the same structure as that found in droplets.[15−19] Other experiments have provided evidence that this kind of structure can also be obtained during recrystallization from high-pressure phases, by heating low-density amorphous ice, by heating glassy aqueous solutions, or by water vapor deposition on cold substrates.[20−23] In the past, this kind of ice was referred to as cubic, with symmetry *Fd*3*m*, or as cubic with hexagonal faults. However, recent studies suggest that what has been called cubic ice in the past does not have a structure consistent with either the cubic crystal system or with the hexagonal crystal system; the experimental diffraction spectra differ from those calculated for cubic ice. Instead, a stacking-disordered ice, I_{sd}, has been introduced recently.[20,24−27] This metastable ice is neither cubic nor hexagonal, and is not a simple mixture of the two, but a combination of cubic sequences intertwined with hexagonal sequences. Moreover, the stacking disorder may vary in complexity depending on the way the ice is formed and on the prevailing thermal conditions during this process.

In this work we present results of X-ray diffraction measurements for ice confined in samples of similar surface

Special Issue: Proceedings of PPEPPD 2016

Received: July 8, 2016
Accepted: November 8, 2016
Published: November 15, 2016

DOI: 10.1021/acs.jced.6b00607
J. Chem. Eng. Data 2016, 61, 4252−4260

chemistry: CMK-3 sample having pores of diameter D = 5.6 nm and two CMK-8 samples having pores of diameters D = 4.8 nm and D = 7.2 nm. The reason for choosing such samples for our studies was the regular rod-like morphology of CMK materials with ordered mesopores and their narrow pore size distribution. The structures of these carbons are inverse replicas of the ordered mesoporous silica and consist of two-dimensional (in the case of CMK-3) or three-dimensional (in the case of CMK-8) arrays of pure carbon nanorods. The pores of these carbons are represented by the void space between regularly spaced nanorods. The pore size of such materials can be tuned (over a the small range) by changing the wall thickness of the silica template. Thus, we were able to synthesize materials with different pore sizes. This allowed us to study how the pore size influenced the melting temperature and the structure of confined ice. It must be noted that the melting behavior of water confined in pores of these types of samples have been investigated by Morishige et al.[7] However, their studies were focused on determination of the pore size dependencies of the freezing and melting temperatures of the confined phase for the pores with several different geometries by means of XRD technique. It was shown that the melting point of frozen water depends on the number of molecules (surface area to volume ratio), not on the pore geometries. In their report, the ice was called cubic with faults without quantitative analysis.

In contrast, the main aspect of our study was the investigation of the pore size dependency of CMK-3 and CMK-8 of the structure of confined ice. Our experiments were conducted by using DSC and XRD techniques. The DSC method was used for determination of the melting points as well as calculation of the melting enthalpies.

In this work, for the first time, we report the formation of stacking-disordered ice, which was identified as having the space group $P3m1$[24] in pores of these types of carbon materials.

EXPERIMENTAL METHODS

Synthesis and Characterization of the Samples. The ordered mesoporous carbon materials of type CMK-3 and CMK-8 were obtained by using SBA-15 and KIT-6 (with different pore diameters), respectively, as templates. The silica matrices were synthesized by following the procedures reported earlier.[28,29] The calcinated products were impregnated with furfuryl alcohol[30] (with acid as catalyst) or glycerol as the carbon source. The as-synthesized composites were subjected to heating at 353 K and then at 433 K in air for 3 h of each temperature. Then the sample was carbonized and subsequently subjected to etching with water−hydrofluoric acid solution and drying.[28]

The materials were characterized by several methods. Small-angle X-ray scattering (SAXS, 2θ from 0° to 5°; transmission setup) and wide-angle XRD (Bragg−Brentano geometry) were carried out on PANalytical's Empyrian diffractometer using Cu $K\alpha_1$ radiation of wavelength 0.154056 nm. Additionally, transmission electron microscopy (HRTEM; Jeol ARM 200F) and nitrogen sorption analysis (Micromeritics ASAP 2020) techniques were used.

The periodicities of the nanostructured samples have been analyzed by using a transmission setup for low-angle diffraction measurement. The generator was operating at 45 kV and 40 mA. The data were collected in a range of 2θ from −0.11° up to 5.0° with a step size of 0.010°. The powder sample was enclosed in circular transmission holders between thin X-ray transparent foils. The background was measured by using an empty sample holder (foil only).

The melting behavior of water confined in the carbon mesopores was studied using DSC and temperature-controlled XRD methods. The melting point in pores was determined by DSC, and the structure of confined ice was analyzed using XRD.

A PerkinElmer DSC 8000 advanced double-furnace differential scanning calorimeter was used to determine the melting temperatures of confined ice by measuring the heat released during the melting process. The range of temperatures was from 173 to 313 K, and the heating rate was 10 K/min. As a result of the DSC experiment, we have obtained a thermogram showing endothermic peaks. These peaks can be characterized by a peak temperature, an onset temperature, and an offset of the thermal event. Because the peak temperature may be shifted due to the heating rate or the sample preparation, we determined the melting temperature from the onset.[31] It is defined as the intersection of the tangent of the peak with the extrapolated baseline. Instead of determining the onset graphically, for better precision, we calculated the derivative of the thermogram. The minimum of the derivative curve corresponds to the onset, because it indicates the place where the argument changes in the fastest way, thus indicating the tangent to the peak. The minimum of the derivative indicates the melting temperature of ice.

The DSC technique was also used for evaluation of the enthalpy change of this transformation. This was done by integrating the area under the DSC peak and dividing the value obtained by the mass of water contained in the pores of the carbon sample. The calculations were performed by incorporation of PerkinElmer's Pyris software.

The structure of the confined ice was investigated using an Empyrean diffractometer equipped with a TTK 450 low-temperature chamber for powder X-ray diffraction studies in reflection geometry. The X-ray diffraction data were acquired in a range of 2θ from 5° to 90° continuously with a step of 0.0066°. Each sample was placed in a capillary tube of 1 mm diameter which was tightly sealed and which was rotated during the experiment. The first X- ray diffraction spectrum was recorded at room temperature (RT). Then the sample was cooled to 173 K and stabilized for 30 min, so that the measurement could be performed. Further measurements on the samples were performed on the heating cycle, at different temperatures below and above the melting temperatures of confined ice inside the pores (as determined by the DSC method). Additionally, the XRD experiment has been performed for bulk H_2O (capillary filled only with water) at temperatures of 173 and 300 K (RT). Also, an empty capillary tube and a capillary filled with a dry carbon sample have been measured in order to exclude their contribution to the final results.

Before the experiment, each of the carbon samples was degassed (heated at 473 K) for several hours in order to remove air and any contamination. In the next step, the sample was placed inside a desiccator, above a container filled with deionized water. The desiccator was sealed after using a prevacuum pump for several minutes. Then, the sample was subjected to a vapor deposition process for several days (3−4). During this process, the mass increment of the sample was monitored. After 3 days, the mass of the sample stopped changing (the pores were fully filled).

DOI: 10.1021/acs.jced.6b00607
J. Chem. Eng. Data 2016, 61, 4252−4260

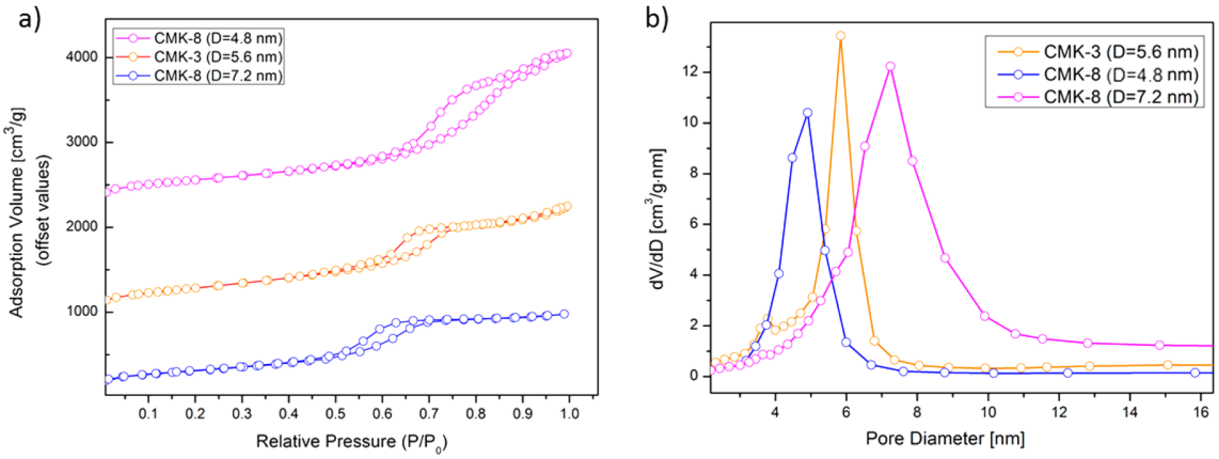

Figure 1. (a) N_2 adsorption−desorption isotherms measured at 77 K, shifted by the values of 1000 cm^3/g for CMK-3 (D = 5.6 nm) and 2000 cm^3/g for CMK-8 (D = 4.8 nm); (b) pore size distribution calculated for the samples.

RESULTS

Characterization of the Pores. Nitrogen adsorption and desorption isotherms were measured at 77 K. The isotherms, which were obtained for both types of samples (Figure 1a), can be classified as being of type IV (according to the IUPAC classification) while the sharp capillary condensation step at high relative pressures is characteristic of a narrow pore size distribution.[43] Also, these isotherms reveal a type H2 adsorption hysteresis loop, which indicates the presence of uniform, interconnected mesopores.[32] According to the literature recommendations[33−36] the specific surface area was calculated by the BET (Brunauer−Emmett−Teller) method, while pore volume and pore size distribution (PSD) were derived by Barrett, Joyner, and Halenda (BJH) method. The results are summarized in Table 1.

Table 1. Summary of N_2 Sorption Analysis Obtained for Mesoporous Carbon Samples

sample	D (nm)[a]	V ($cm^3\ g^{-1}$)[b]	S_{BET} ($m^2\ g^{-1}$)[c]
CMK-3	5.6	1.83	1211
CMK-8	4.8	2.00	1327
CMK-8	7.2	2.96	1361

[a]D = pore diameter. [b]V = pore volume. [c]S_{BET} = specific surface area.

The results of the small-angle X-ray scattering pattern confirm that the structure of the carbon sample is regular. For CMK-3 (Figure 2a), three well-resolved peaks are observed, indexed as (100), (110), and (200), which are associated with hexagonally arranged carbon nanorods belonging to space group *P6mm*. In the case of CMK-8 (Figure 2b), the XRD peaks (211) and (220) can be assigned to the structure with cubic *Ia3d* symmetry.[32] The regular structures of CMK-3 and CMK-8 are also confirmed in TEM micrographs (Figure 2c,e, respectively).

In addition, the experimental curve obtained from the wide-angle XRD experiment exhibits (Figure 2d) two broad peaks: the first one, (002), results from stacks of parallel layer planes at 2θ = 23°, and the second one, (101), results from the regular structure within the individual layer plane segments at 2θ = 43.4°. These types of reflections are characteristic for the carbon clusters, which consist of small fragments of graphene planes and also of some disordered carbon.[37]

DSC Results. DSC measurements were performed in order to determine the melting temperature of confined ice in each sample: CMK-8 (D = 4.8 nm), CMK-3 (D = 5.6 nm), and CMK-8 (D = 7.2 nm). In Figure 3, we show the DSC thermogram representing the melting process of ice located inside the pores of the sample CMK-3 of 5.6 nm diameter. The endothermic peak occurs at a temperature of ∼256.8 K which corresponds to the melting temperature of the confined ice. The ice−water phase transition shift, with respect to the phase transition of bulk ice, is thus $\Delta T = T_{mb} - T_{mp} = -16.5$ K (where T_{mb} and T_{mp} stand for melting temperature of bulk ice and melting temperature of confined ice, respectively). The absence of an endothermic peak at a temperature of 273 K proves that there is no bulk H_2O in the sample. Gray circles on the DSC curve indicate the temperature points at which the XRD measurements were performed.

The DSC results obtained for all three samples are presented in Figure 4. On each DSC curve only one endothermic peak appears, and because it happens at temperatures below 273 K, it is associated with the solid−liquid transition of confined ice. The melting points have been determined from the derivatives (as shown in Figure 3), and they are summarized in Table 2. The DSC results indicate that the smaller the pore size is of the constricting sample, the lower the melting temperature of confined ice. This dependency is presented in Figure 5 where the phase transition shift is plotted as a function of the reciprocal of the pore diameter $1/D$.

For sufficiently large pores, the melting behavior of confined substances can be described by the Gibbs−Thomson equation of classical thermodynamics,[39,40] which predicts that the shift of the melting point is given by

$$\frac{T_{mp} - T_{mb}}{T_{mb}} = \frac{1(\gamma_{WS} - \gamma_{WL})\nu_L}{D\lambda_b} \quad (1)$$

where γ is interfacial tension, ν_L is the molar volume of the bulk liquid (water here), and λ_b is the latent heat of melting of the bulk liquid water; W, S, and L refer to the pore wall, solid ice on the pore wall, and liquid water on the pore wall, respectively. Equation 1 does not account for the effect of the wall forces at the nanoscale but is expected to be valid for very large pores. Equation 1 predicts that a plot of $(T_{mp} - T_{mb})$ versus inverse pore diameter should be linear. However, as seen in Figure 5 the Gibbs−Thomson equation breaks down for smaller pores

DOI: 10.1021/acs.jced.6b00607
J. Chem. Eng. Data 2016, 61, 4252−4260

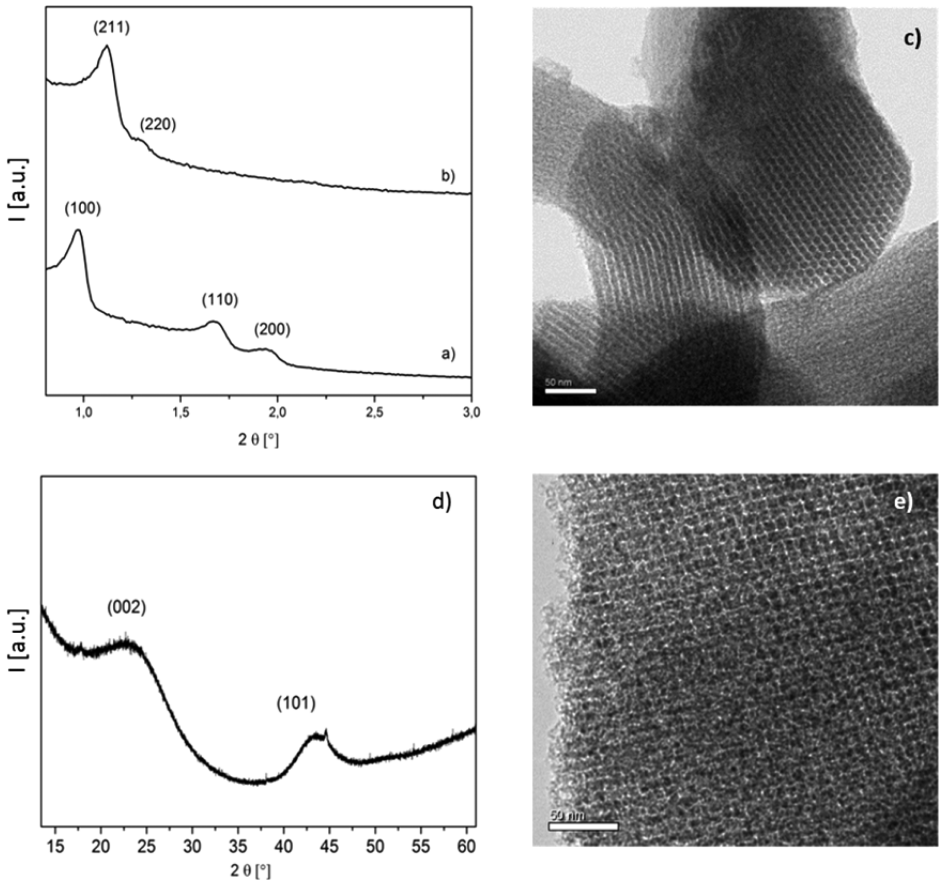

Figure 2. Results of the characterization of ordered mesoporous carbon samples: (a) small-angle XRD patterns obtained for CMK-3; (b) small-angle XRD patterns obtained for CMK-8; (c) transmission electron microscopy image of CMK-3; (d) wide-angle XRD diffraction for CMK-8; (e) transmission electron microscopy image of CMK-8.

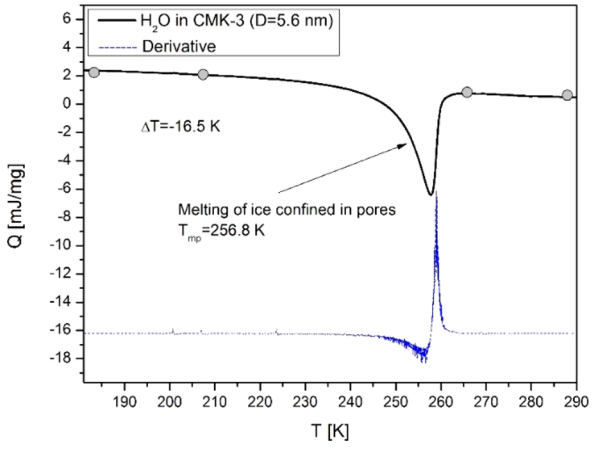

Figure 3. DSC scan for H_2O in CMK-3 and its derivative. Gray circles indicate the temperatures at which the XRD measurements were performed.

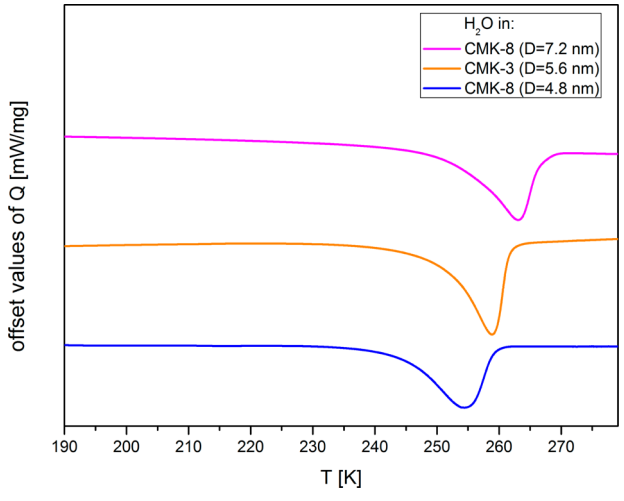

Figure 4. DSC scans obtained for H_2O confined in pores of different carbon samples.

and is in serious error for pore diameter below 10 nm (about 32 molecular diameters). Similar results showing the breakdown of the Gibbs−Thomson equation have been reported[38] for other adsorbate−adsorbant systems.

The values of enthalpy changes, ΔH, for the melting transition of ice located in pores of carbon samples were determined. The values of ΔH calculated for ice located inside carbon mesopores for CMK-8 (D = 4.8 nm), CMK-3 (D = 5.6 nm), and CMK-8 (D = 7.2 nm) are 1.2; 1.2, and 1.4 kJ mol^{-1}, respectively (see also Table 2). These values differ from the values of the enthalpy change for the hexagonal ice−liquid transition (ΔH_h = 6.01 kJ mol^{-1}) and the enthalpy change for the cubic−hexagonal transition (ΔH_c), which vary from 23 to 160 J mol^{-1},[21,22,41] and suggest the existence of the ice−liquid transitions between a novel, well-defined ice structure and liquid.

DOI: 10.1021/acs.jced.6b00607
J. Chem. Eng. Data 2016, 61, 4252−4260

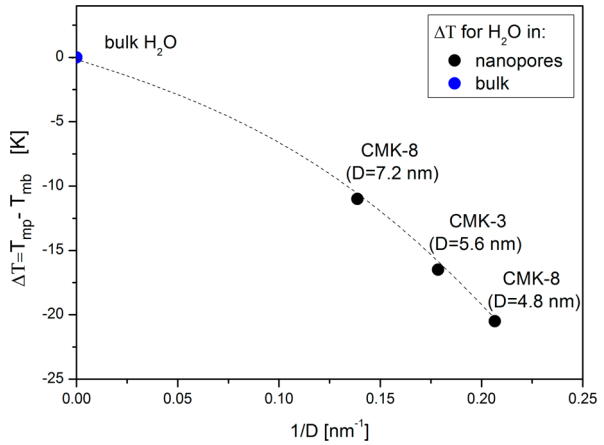

Figure 5. Melting temperature shift of ice with respect to the melting point for bulk ice as a function of 1/D.

RESULTS AND ANALYSIS OF XRD MEASUREMENTS

For analysis of the structure of ice confined in CMK-3 (D = 5.6 nm) and two samples of CMK-8 (D = 4.8 nm and D = 7.2 nm, respectively), the temperature-controlled wide-angle XRD method was used. The wide-angle XRD results for the empty capillary and the dry carbon sample, obtained at temperatures 173 K and RT, are presented in Figure 6. As follows from

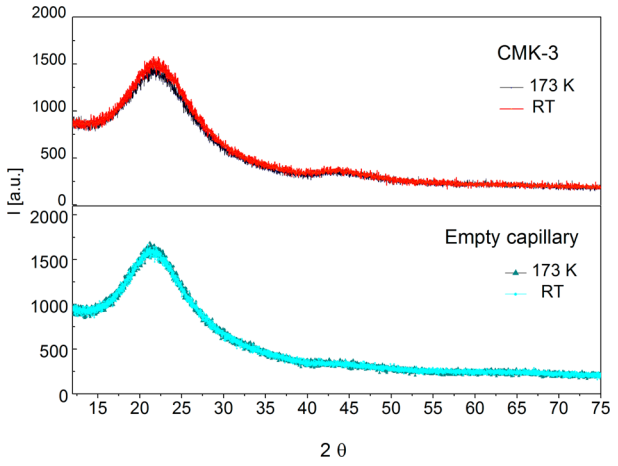

Figure 6. X-ray diffraction results for the empty capillary tube and for the capillary filled with dry CMK-3, measured at temperatures 173 and 300 K (RT).

Figure 6, the experimental curves do not change significantly over the whole range of temperature. In each case, there is a maximum visible in the range 2θ = 20−40°, which originates from the amorphous structure of the borosilicate walls of the capillary, which dominates for the carbon samples.

The XRD results for bulk H_2O (capillary filled with water) are presented in Figure 7. The diffraction pattern obtained at 173 K (purple color) has been compared with the database ICDD (PDF No. 00-42-1141; green color). The positions and the relative intensities of the peaks obtained are consistent with the reference pattern; bulk ice possesses hexagonal symmetry ($P6_3/mm$). The same sample was also measured at RT. In this case the crystalline peaks were not observed. Only a large bump was visible in the range from 15° to 50°, which is typical for the liquid state.

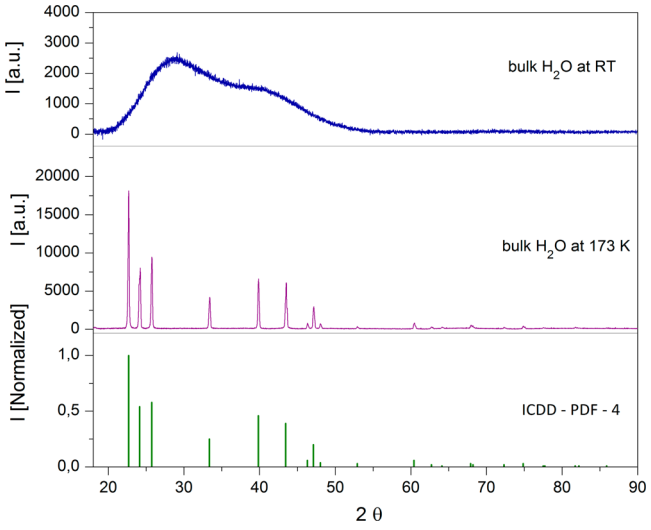

Figure 7. XRD spectra for H_2O obtained at temperatures RT (dark blue) and 173 K (purple) compared to the reference pattern for hexagonal ice (green).

The results of the XRD experiment obtained for ice confined in CMK-3 (5.6 nm), are shown in Figure 8. The measurements were performed at temperatures 173, 213, and 268 K and at RT. Different colors are given to the experimental curves corresponding to the temperatures at which measurements were taken. The dashed pink line indicates the melting temperature of the confined ice, determined by the DSC method.

As seen from Figure 8, clear crystalline patterns are observed in the case of data which were recorded at temperatures of 173 and 213 K, that is, at temperatures which correspond to the solid phase of H_2O contained inside the pores of CMK-3 (D = 5.6 nm). Both of these XRD patterns are the same, which indicates that the structure of ice is stable in this range of temperatures. On the other hand, none of these diffraction peaks are observed at temperatures above T_{mp} = 256.8 K, which indicates that the ice melted, in agreement with the DSC measurements. It can be concluded that the XRD patterns obtained at temperatures 173 and 213 K refer only to the confined ice inside the pores of the sample. For further structural analysis, the diffraction pattern obtained at the temperature of 173 K was chosen.

Analysis of the XRD data was performed by incorporation of PANalytical's High Score Plus software. The intensities and the peak positions of the resulting XRD patterns are presented in Figure 9a. As can be seen, there are three main peaks at positions of 22.79°, 24.21°, and 25.80° (marked with the orange lines). According to the database ICDD (PDF No. 00-42-1141) these peaks can be assigned to the (100), (002), and (101) planes in a hexagonal crystalline structure (green color). The reference peaks for this hexagonal structure ($P6/mm$) according to this database should have relative intensities following the order 100%, 54%, and 58%, respectively. In our experimental data, however, the relative intensities are 52.63%, 100%, and 15.76% for the corresponding aforementioned crystalline peaks.

The shift in relative intensity suggests the existence of a secondary phase of ice in the sample. The peak position of the cubic form coincides with lines of the hexagonal structure. Therefore, in a mixture of these two phases, the cubic form can be found only by analysis of the ratio of the peak intensities.

DOI: 10.1021/acs.jced.6b00607
J. Chem. Eng. Data 2016, 61, 4252−4260

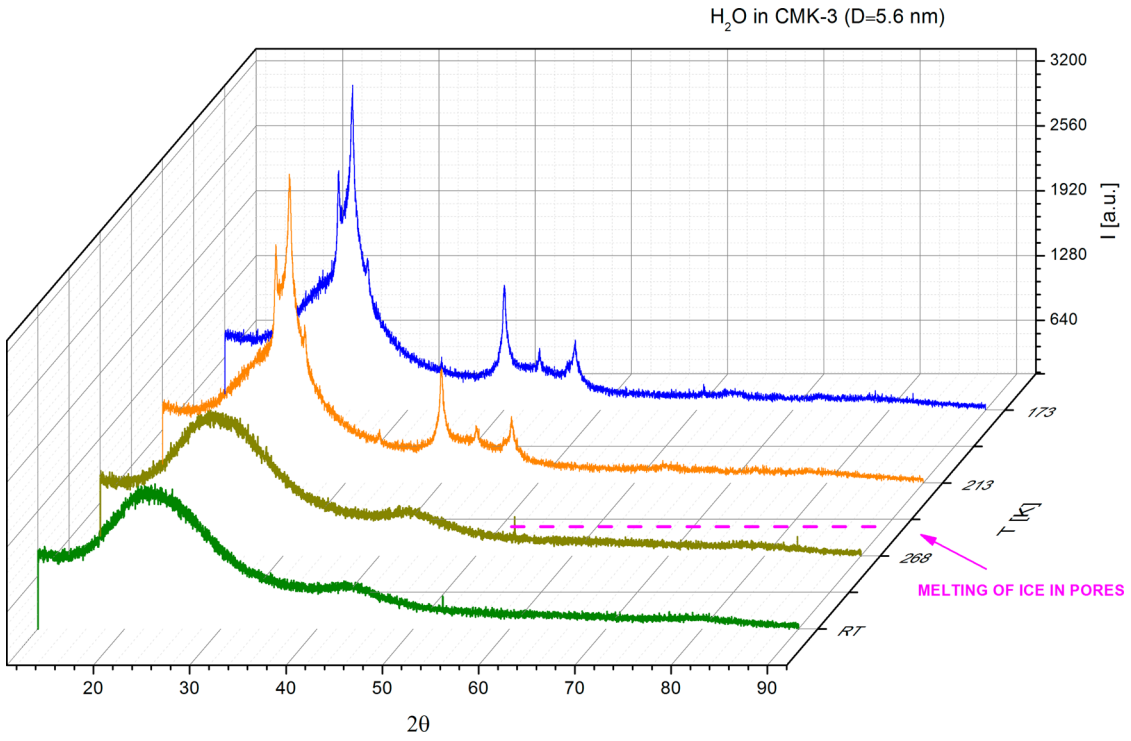

Figure 8. XRD spectrum for H_2O confined inside the pores of CMK-3 (D = 5.6 nm) measured at different temperatures. The dashed line indicates the melting temperature of confined ice (determined by DSC method).

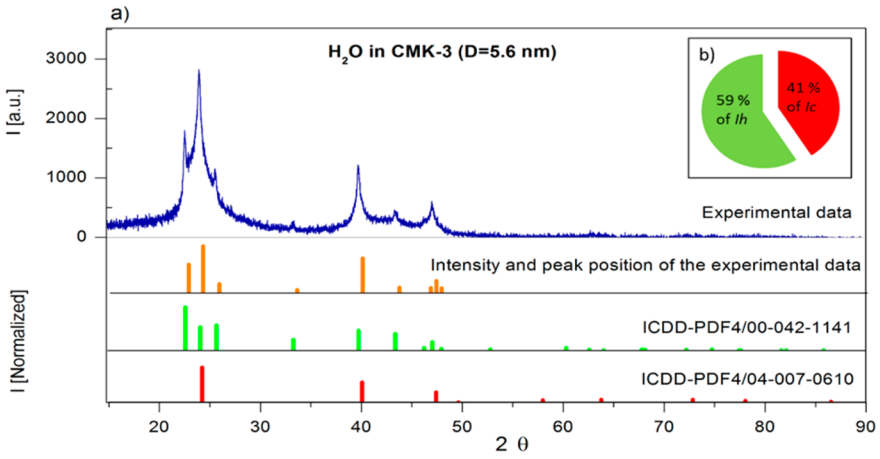

Figure 9. (a) Intensity and peak positions of the experimental XRD patterns obtained for H_2O in CMK-3 (D = 5.6 nm) at 173 K (orange), and the positions of the peaks for hexagonal (green) and cubic (red) ice structures, respectively; (b). quantification of the hexagonal and cubic ice fractions calculated by using PANalytical's Highscore Plus software.

The analysis was performed with accordance to the literature recommendation.[15,24,42] As follows from the database ICDD (PDF No. 04-007-0610), a peak which appears at 24.22° is the most intense in the spectrum (Figure 9a, red color) and can be assigned to the (111) plane of the cubic structure with the space group *Fd*3*m*.[42] The software HighScore Plus was used to carefully fit both intensities and peak positions and to assess the contribution of hexagonal ice and cubic ice in the investigated sample. As a result, it was concluded that the ice confined in pores of CMK-3 (D = 5.6 nm) contains a mixture of 59% hexagonal ice and 41% cubic ice, with no other crystalline phases present.

The structure of the ice formed inside pores of the other carbon samples were analyzed in the same way. The results obtained for ice in CMK-8 (D = 4.8 nm) and CMK-8 (D = 7.2 nm) are presented in Figure 10 and Figure 11, respectively.

All of the experimental curves present well-resolved diffraction patterns, which vary between each other, suggesting the coexistence of a different combination of I_c and I_h. In general, the higher the intensity of the peak is at position 24.22° with respect to those at 22.7° and 25.83° positions, the greater the content of I_c in the ice crystal.

The calculated content of I_c and I_h for each of the samples, and the corresponding values of the melting points (which have been determined from the derivatives), are summarized in Table 2.

It seems that in the case of ice formed inside pores of CMK-3 and CMK-8 samples, the quantity of cubic ice I_c increases when the pore diameter gets smaller. In order to visualize this

DOI: 10.1021/acs.jced.6b00607
J. Chem. Eng. Data 2016, 61, 4252−4260

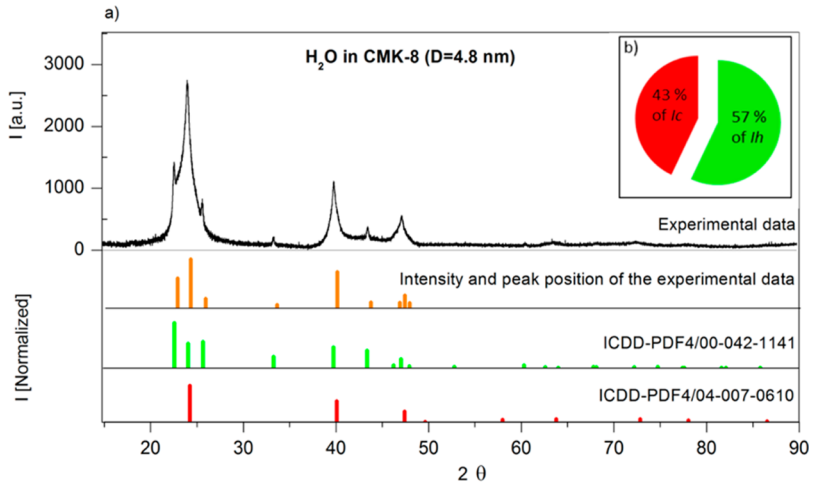

Figure 10. (a) Intensity and peak positions of the experimental XRD patterns obtained for H_2O in CMK-8 (D = 4.8 nm) at 173 K (orange), and positions of the peaks for hexagonal (green) and cubic (red) ice structures, respectively; (b) quantification of the hexagonal and cubic ice fractions calculated by using PANalytical's Highscore Plus software.

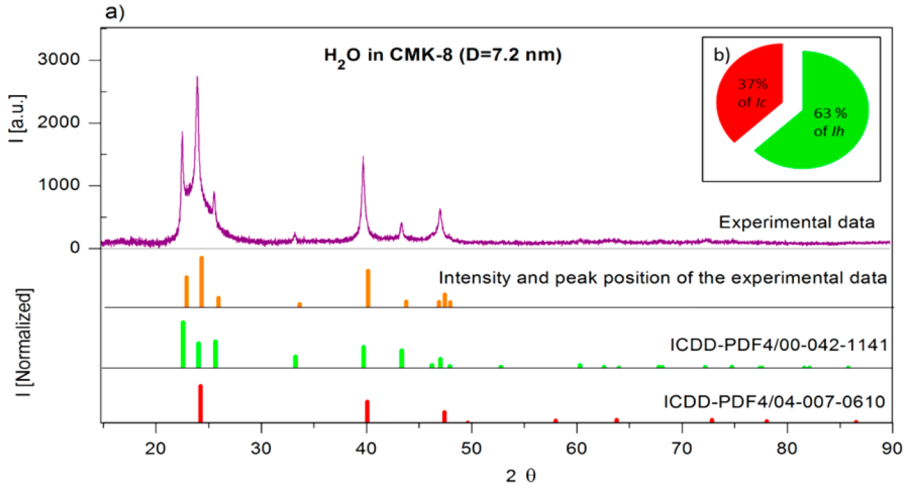

Figure 11. (a) Intensity and peak positions of the experimental XRD patterns obtained for H_2O in CMK-8 (D = 7.2 nm) at 173 K (orange), and positions of the peaks for hexagonal (green) and cubic (red) ice structures, respectively; (b) quantification of the hexagonal and cubic ice fractions calculated by using PANalytical's Highscore Plus software.

Table 2. Melting Temperature Shift of Confined Ice and the Percentage Composition of Phases (Cubic and Hexagonal Ice) Depending on the Pore Size of the Sample

			composition (%)		
carbon sample	D (nm)	ΔT_{mp} (K)	I_c	I_h	ΔH (kJ mol^{-1})]
CMK-8	4.84	−20.5	43	57	1.2
CMK-3	5.6	−16.5	41	59	1.2
CMK-8	7.21	−11	37	63	1.4

dependency, the calculated values of I_c content in each sample have been plotted against their pore width, D (Figure 12). Also, the I_c content as a function of ΔT is presented in Figure 13. Similar dependences were obtained by Morishige et al., who studied the structure of ice confined in cylindrical silica nanopores of various pore sizes.[44]

Based on our experimental results, we can confirm that the solid phase of ice formed inside the nanopores possesses a complicated structure, different from that of bulk ice. However, we can only approximately assess the quantity of these two fractions.

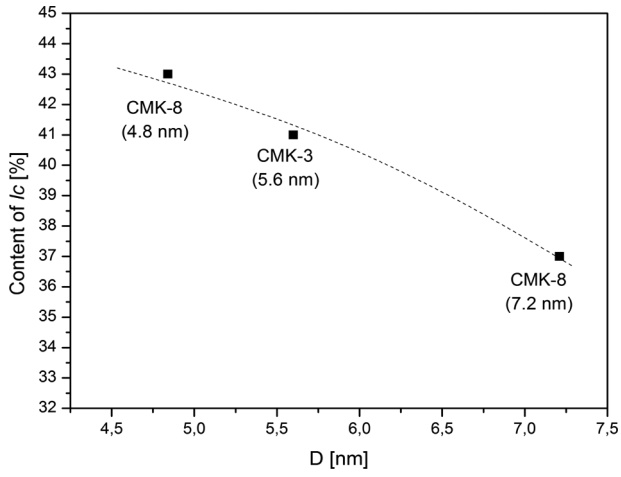

Figure 12. Content of cubic ice I_c in the confined ice versus D.

DOI: 10.1021/acs.jced.6b00607
J. Chem. Eng. Data 2016, 61, 4252−4260

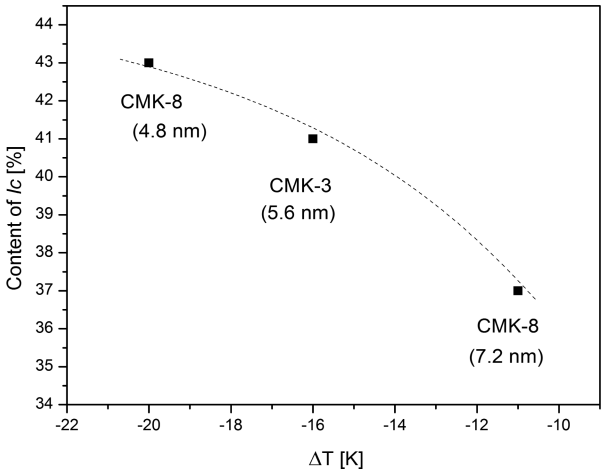

Figure 13. Content of cubic ice I_c in the confined ice versus ΔT.

In the bulk phase at ambient pressure ice has been observed to exist in two crystalline forms: stable hexagonal ice I_h and metastable cubic ice I_c. While the stable hexagonal ice is the most common crystal form occurring in the bulk phase below 273 K, the structure of the metastable form of bulk ice seems to be still ambiguous. Morishige et al. suggested that this form of ice may be composed of very small crystallites of hexagonal ice that contains a large amount of growth faults, depending on the crystallite size; that is, ice with disordered stacking sequence.[44] Recently, Malkin et al.[24] argued that what has been called cubic ice in the past does not have a structure consistent with the cubic crystal system. Instead, their new theory predicts that when a water droplet freezes, a two-dimensional nucleation process occurs. As a result, the layers of hexagonal and cubic ice structures grow alternately in the crystal (in various combinations), so the resulting ice is made up of a combination of intertwined cubic and hexagonal stacking sequences. Such a solid is not just a simple binary mixture consisting of I_h and I_c fractions and does not possess either cubic or hexagonal symmetry.[20,24,26,27,44] Recently the existence of disordered ice was reported for water in nanoporous and alumina.[45] The name proposed for this complex structure was proposed disordered stacking ice, I_{sd}. It was also found[24] that when water droplets freeze at a lower temperature, the resultant ice possesses a higher fraction of the cubic sequences. This is a consequence of in-layer competition between hexagonal and cubic stacks during cross-nucleation. It was hypothesized that ice which initially forms at higher temperatures is also stacking-disordered, but freezing at these conditions can provide an opportunity for the ice to anneal, leading to ice which is structurally closer to ice I_h.

In our results reported here we find a depression of the freezing/melting temperature of water due to confinement, with this effect becoming more pronounced as the pore diameter is reduced. At the same time, this decrease in the transition temperature with decreasing pore size is accompanied by an increase in the proportion of cubic ice, I_c (Table 2 and Figures 12 and 13). This finding appears to be in accord with the proposal of Malkin et al.,[24] that when freezing occurs at a higher temperature (larger pores in our case), an annealing process can occur, leading to ice possessing more $I_h$sequences.

CONCLUSIONS

Our DSC studies indicate a reduction in the melting temperature of water due to confinement in the pores of the ordered carbons CMK-3 and CMK-8, the effect becoming more pronounced as the pore diameter decreases. The results show that the Gibbs−Thomson equation breaks down for smaller pores and is in serious error for pore diameters below about 10 nm. Similar results showing the breakdown of the Gibbs−Thomson equation have been reported[38] for other adsorbate−adsorbent systems.

Wide-angle X-ray scattering measurements for these systems were made for temperatures below the bulk melting point. For temperatures below the pore melting temperature the diffraction spectra showed features of both hexagonal ice, I_h, and cubic ice, I_c. We were able to assess quantitatively the relative contributions of I_c and I_h by analysis of the experimental data with the patterns listed in the database HighScore. Our results indicate the existence of disordered stacking ice, I_{sd}, in the pores and show that the proportion of I_c increases as the pore diameter is reduced. This observation appears to be consistent with that by Malkin et al.,[24] who found a similar increase in ice I_c in liquid water drops as the freezing temperature was reduced.

AUTHOR INFORMATION

Corresponding Author

*E-mail:msb@amu.edu.pl.

Funding

Financial support from the National Centre for Research and Development under research grant "Nanomaterials and their application to biomedicine", Contract No. PBS1/A9/13/2012, is gratefully acknowledged. We thank the National Center of Science under Grant DEC-2013/09/B/ST4/03711; K.E.G. thanks the U.S. National Science Foundation for a grant (CBET-1160151) in support of this work. Also, this work was supported by the International Ph.D. Projects Programme of the Foundation for Polish Science operated within the Innovative Economy Operational Programme (IE OP) 2007−2013 within European Regional Development Fund.

Notes

The authors declare no competing financial interest.

ACKNOWLEDGMENTS

We are grateful to M. Kempka for his kind help with the sample degassing and E. Coy for his kindness and help with the analysis of the structure of ice.

REFERENCES

(1) Gelb, L. D.; Gubbins, K. E.; Radhakrishnan, R.; Sliwinska-Bartkowiak, M. Phase Separation in Confined Systems. *Rep. Prog. Phys.* **1999**, *62*, 1573−1659.

(2) Radhakrishnan, R.; Gubbins, K. E.; Sliwinska-Bartkowiak, M. Global Phase Diagrams for Freezing in Porous Media. *J. Chem. Phys.* **2002**, *116*, 1147.

(3) Alba-Simionesco, C.; Coasne, B.; Dosseh, G.; Dudziak, G.; Gubbins, K. E.; Radhakrishnan, R.; Sliwinska-Bartkowiak, M. Effects of Confinement on Freezing and Melting. *J. Phys.: Condens. Matter* **2006**, *18*, R15−R68.

(4) Sliwinska-Bartkowiak, M.; Dudziak, G.; Sikorski, R.; Gras, R.; Radhakrishnan, R.; Gubbins, K. E. Melting/freezing Behavior of a Fluid Confined in Porous Glasses and MCM-41: Dielectric Spectroscopy and Molecular Simulation. *J. Chem. Phys.* **2001**, *114*, 950.

(5) Steytler, D. C.; Dore, J. C.; Wright, C. J. Neutron Diffraction Study of Cubic Ice in a Porous Silica Network. *J. Phys. Chem.* **1983**, *87*, 2458−2459.

(6) Morishige, K.; Yasunaga, H.; Uematsu, H. Stability of Cubic Ice in Mesopores. *J. Phys. Chem. C* **2009**, *113*, 3056−3061.

DOI: 10.1021/acs.jced.6b00607
J. Chem. Eng. Data 2016, 61, 4252−4260

(7) Morishige, K.; Yasunaga, H.; Matsutani, Y. Effect of Pore Shape on Freezing and Melting Temperatures of Water. *J. Phys. Chem. C* **2010**, *114*, 4028−4035.
(8) Liu, K.-H.; Zhang, Y.; Lee, J.-J.; Chen, C.-C.; Yeh, Y.-Q.; Chen, S.-H.; Mou, C.-Y. Density and Anomalous Thermal Expansion of Deeply Cooled Water Confined in Mesoporous Silica Investigated by Synchrotron X-Ray Diffraction. *J. Chem. Phys.* **2013**, *139*, 064502.
(9) Jazdzewska, M.; Sliwinska-Bartkowiak, M. M.; Beskrovnyy, A. I.; Vasilovskiy, S. G.; Ting, S.-W.; Chan, K.-Y.; Huang, L.; Gubbins, K. E. Novel Ice Structures in Carbon Nanopores: Pressure Enhancement Effect of Confinement. *Phys. Chem. Chem. Phys.* **2011**, *13*, 9008−9013.
(10) Koga, K.; Gao, G. T.; Tanaka, H.; Zeng, X. C. Formation of Ordered Ice Nanotubes inside Carbon Nanotubes. *Nature* **2001**, *412*, 802−805.
(11) Lei, Z.; Bai, S.; Xiao, Y.; Dang, L.; An, L.; Zhang, G.; Xu, Q. CMK-5 Mesoporous Carbon Synthesized via Chemical Vapor Deposition of Ferrocene as Catalyst Support for Methanol Oxidation. *J. Phys. Chem. C* **2008**, *112*, 722−731.
(12) Takaiwa, D.; Hatano, I.; Koga, K.; Tanaka, H. Phase Diagram of Water in Carbon Nanotubes. *Proc. Natl. Acad. Sci. U. S. A.* **2008**, *105*, 39−43.
(13) Maniwa, Y.; Kataura, H.; Abe, M.; Udaka, A.; Suzuki, S.; Achiba, Y.; Kira, H.; Matsuda, K.; Kadowaki, H.; Okabe, Y. Ordered Water inside Carbon Nanotubes: Formation of Pentagonal to Octagonal Ice-Nanotubes. *Chem. Phys. Lett.* **2005**, *401*, 534−538.
(14) Johari, G. P. Water's Size-Dependent Freezing to Cubic Ice. *J. Chem. Phys.* **2005**, *122*, 194504.
(15) Murray, B. J.; Knopf, D. A.; Bertram, A. K. The Formation of Cubic Ice under Conditions Relevant to Earth ' S Atmosphere. *Nature* **2005**, *434*, 202−205.
(16) Murray, B. J.; Jensen, E. J. Homogeneous Nucleation of Amorphous Solid Water Particles in the Upper Mesosphere. *J. Atmos. Sol.-Terr. Phys.* **2010**, *72*, 51−61.
(17) Whalley, E. Cubic Ice in Nature. *J. Phys. Chem.* **1983**, *87*, 4174−4179.
(18) Murray, B. J.; Bertram, A. K. Formation and Stability of Cubic Ice in Water Droplets. *Phys. Chem. Chem. Phys.* **2006**, *8*, 186−192.
(19) Arnold, G. P. Neutron-Diffraction Study of Ice Polymorphs. III. Ice Ic. *J. Chem. Phys.* **1968**, *49* (10), 4365.
(20) Hansen, T. C.; Koza, M. M.; Lindner, P.; Kuhs, W. F. Formation and Annealing of Cubic Ice: II. Kinetic Study. *J. Phys.: Condens. Matter* **2008**, *20*, 285105.
(21) Shilling, J. E.; Tolbert, M. a.; Toon, O. B.; Jensen, E. J.; Murray, B. J.; Bertram, A. K. Measurements of the Vapor Pressure of Cubic Ice and Their Implications for Atmospheric Ice Clouds. *Geophys. Res. Lett.* **2006**, *33*, L17801.
(22) Kohl, I.; Mayer, E.; Hallbrucker, A. The Glassy Water − Cubic Ice System: A Comparative Study by X-Ray Difraction and Differential Scanning Calorimetry. *Phys. Chem. Chem. Phys.* **2000**, *2*, 1579−1586.
(23) Kumai, M.*A Study of Hexagonal and Cubic Ice at Low Temperatures*, Research Report 231; Cold Regions Research & Engineering Laboratory, U.S. Army Materiel Command: Hanover, NH, USA, 1967.
(24) Malkin, T. L.; Murray, B. J.; Salzmann, C.; Molinero, V.; Pickering, S. J.; Whale, T. F. Stacking Disorder in Ice I. *Phys. Chem. Chem. Phys.* **2015**, *17*, 60−76.
(25) Malkin, T. L.; Murray, B. J.; Brukhno, A. V.; Anwar, J.; Salzmann, C. G. Correction for Malkin et al., Structure of Ice Crystallized from Supercooled Water. *Proc. Natl. Acad. Sci. U. S. A.* **2012**, *109*, 4020.
(26) Moore, E. B.; Molinero, V. Is It Cubic? Ice Crystallization from Deeply Supercooled Water. *Phys. Chem. Chem. Phys.* **2011**, *13*, 20008−20016.
(27) Kuhs, W. F.; Sippel, C.; Falenty, A.; Hansen, T. C. Extent and Relevance of Stacking Disorder in "Ice I(c). *Proc. Natl. Acad. Sci. U. S. A.* **2012**, *109*, 21259−21264.
(28) Jun, S.; Joo, S. H.; Ryoo, R.; Kruk, M.; Jaroniec, M.; Liu, Z.; Ohsuna, T.; Terasaki, O. Synthesis of New, Nanoporous Carbon with Hexagonally Ordered Mesostructure. *J. Am. Chem. Soc.* **2000**, *122*, 10712−10713.
(29) Kleitz, F.; Choi, S. H.; Ryoo, R. Cubic *Ia*3*d* Large Mesoporous Silica: Synthesis and Replication to Platinum Nanowires, Carbon Nanorods and Carbon Nanotubes. *Chem. Commun.* **2003**, 2136−2137.
(30) Li, F.; Morris, M.; Chan, K. Electrochemical Capacitance and Ionic Transport in the Mesoporous Shell of a Hierarchical Porous Core-Shell Carbon Structure. *J. Mater. Chem.* **2011**, *21*, 8880−8886.
(31) Zhao, J.*Methods for Phase Diagram Determination*; Elsevier Science: Amsterdam, 2007.
(32) Lu, A.-H.; Dongyuan, Z.; Wan, Y.; O'Brien, P.; Craighead, H.; Kroto, H.*Nanocasting: A Versatile Nanostructured Strategy for Creating Porous Materials*; RSC Nanoscience and Nanotechnology; ;Royal Society of Chemistry: Cambridge, U.K., 2010.
(33) Lezanska, M.; Wloch, J.; Szymanski, G.; Szpakowska, I.; Kornatowski, J. Properties of CMK-8 Carbon Replicas Obtained from KIT-6 and Pyrrole at Various Contents of Ferric Catalyst. *Catal. Today* **2010**, *150*, 77−83.
(34) Saikia, D.; Wang, T.; Chou, C.; Fang, J.; Tsai, L.; Kao, H. A Comparative Study of Ordered Mesoporous Carbons with Different Pore Structures as Anode Materials for Lithium-Ion Battieries. *RSC Adv.* **2015**, *5*, 42922−42930.
(35) Thao, N. T. Synthesis and Characterization of Carbon Molecular Sieve. *VNU J. Sci., Nat. Sci. Technol.* **2011**, *27*, 259−263.
(36) Indrawirawan, S.; Sun, H.; Duan, X.; Wang, S. Applied Catalysis B: Environmental Nanocarbons in Different Structural Dimensions (0 − 3D) for Phenol Adsorption and Metal-Free Catalytic Oxidation. *Appl. Catal., B* **2015**, *179*, 352−354.
(37) Kim, P.; Joo, J. B.; Kim, J.; Kim, W.; Song, I. K.; Yi, J. Sucrose-Derived Graphitic Porous Carbon Replicated by Mesoporous Silica. *Korean J. Chem. Eng.* **2006**, *23*, 1063−1066.
(38) Gubbins, K. E.; Long, Y.; Śliwinska-Bartkowiak, M. Thermodynamics of Confined Nano-Phases. *J. Chem. Thermodyn.* **2014**, *74*, 169−183.
(39) Sliwinska-Bartkowiak, M.; Gras, J.; Sikorski, R.; Radhakrishnan, R.; Gelb, L.; Gubbins, K. E. Phase Transitions in Pores: Experimental and Simulation Studies of Melting and Freezing. *Langmuir* **1999**, *15*, 6060−6069.
(40) Evans, R.; Marini Bettolo Marconi, U. Phase Equilibria and Solvation Forces for Fluids Confined between Parallel Walls. *J. Chem. Phys.* **1987**, *86*, 7138.
(41) Murphy, D. M. Dehydration in Cold Clouds Is Enhanced by a Transition from Cubic to Hexagonal Ice. *Geophys. Res. Lett.* **2003**, *30*, 2230.
(42) Dowell, L. G.; Moline, W. S.; Rinfret, P. A. A Low-Temperature X-Ray Diffraction Study Of Ice Structures Formed in Aqueous Gelation Gels. *Biochim. Biophys. Acta* **1962**, *59*, 158−167.
(43) Rouquerol, J.; Avnir, D.; Fairbridge, W. C.; Everett, D. H.; Haynes, J. H.; Pernicone, N.; Ramsay, J. D. F.; Sing, K. S. W.; Unger, K. K. Recommendations for the Characterization of Porous Solids. *J. Pure Appl. Chem.* **1994**, *66*, 1739−1758.
(44) Morishige, K.; Uematsu, H. The Proper Structure of Cubic Ice Confined in Mesopores the Proper Structure of Cubic Ice Confined in Mesopores. *J. Chem. Phys.* **2005**, *122*, 044711.
(45) Suzuki, Y.; Duran, H.; Steinhart, M.; Kappl, M.; Butt, H.-J.; Floudas, G. Homogeneous Nucleation of Predominantly Cubic Ice Confined in Nanoporous Alumina. *Nano Lett.* **2015**, *15*, 1987−1992.

DOI: 10.1021/acs.jced.6b00607
J. Chem. Eng. Data 2016, 61, 4252−4260